

Article

A Simulation Study of FRP-PCM Reinforcement for Tunnel Linings with Void Defects

Qiwei Lin ^{1,*}, Yujing Jiang ¹ , Jing Wang ² and Satoshi Sugimoto ¹

¹ Graduate School of Engineering, Nagasaki University, Nagasaki 852-8521, Japan; jiang@nagasaki-u.ac.jp (Y.J.); s-sugi@nagasaki-u.ac.jp (S.S.)

² MCC Wukan Engineering Technology Co., Ltd., Wuhan 430080, China; wjwayne03@163.com

* Correspondence: linqiweilink@163.com

Abstract: Voids behind tunnel linings can be formed either during or after the construction phase, occurring due to inadequate backfilling, substandard workmanship, water erosion, or gravitational forces. Investigations into numerous tunnels in which collapses occurred while in operation have indicated that voids behind the liner constitute the primary contributors to these failures. Consequently, it is imperative to devise lining reinforcement strategies tailored to the specific conditions encountered in the field. Fiber-reinforced plastic (FRP) represents a viable alternative construction material that has been widely utilized in the reinforcement of concrete structures. It is essential to quantitatively assess the reinforcing effect of FRP grids when they are employed in the restoration of deteriorated tunnel linings, thereby facilitating the development of effective maintenance designs. In this study, we aimed to enhance the sensitivity analysis of the reinforcement method by evaluating the impact of voids through the analysis of bending moments and axial forces within the tunnel lining. The effects of voids based on the different locations in which they occur were explored numerically through an Elastoplast finite element analysis. The study involved simulating tunnel linings that had been reinforced with FRP grids and assessing the effects of such reinforcement in tunnels afflicted with various structural problems. Based on the outcomes of these simulations, the internal forces within the lining are scrutinized, and the efficacy of the reinforcement is appraised.

Keywords: tunnel defect; lining; voids; insufficient thickness; framed structure analysis



Citation: Lin, Q.; Jiang, Y.; Wang, J.; Sugimoto, S. A Simulation Study of FRP-PCM Reinforcement for Tunnel Linings with Void Defects. *Appl. Sci.* **2024**, *14*, 9440. <https://doi.org/10.3390/app14209440>

Academic Editor: Syed Minhaj Saleem Kazmi

Received: 20 September 2024

Revised: 11 October 2024

Accepted: 15 October 2024

Published: 16 October 2024



Copyright: © 2024 by the authors. Licensee MDPI, Basel, Switzerland. This article is an open access article distributed under the terms and conditions of the Creative Commons Attribution (CC BY) license (<https://creativecommons.org/licenses/by/4.0/>).

1. Introduction

Numerous mountain tunnels in Japan were constructed expeditiously during the era of robust economic expansion, and these structures have now been operational for periods ranging from 30 to 50 years [1]. The conditions of many of these tunnels are not promising, with varying degrees of structural deficiencies manifesting. Many researchers have concentrated their studies on voids situated behind the lining structures of tunnels. The determinants influencing these voids encompass the location, depth, and dimensions of the voids themselves [2]. The effects of these factors on the mechanical behavior of the lining have been extensively examined through a multitude of methodologies. Numerous studies have concentrated on analyzing the mechanical behavior of tunnel linings, particularly under the influence of void defects [3]. Theoretical analyses of tunnel lining behavior have been extensively conducted using approaches such as the Hoek–Brown failure criterion and classical calculus of variations techniques to assess stress and failure conditions [4]. These analyses confirm correlations from a theoretical perspective, and derive three-dimensional elastic solutions for a deep cylindrical tunnel with a void subjected to obliquely incident seismic waves [5]. Furthermore, empirical field investigations have provided crucial insights. These studies have been performed utilizing methods such as microtremor analysis to assess tunnel health conditions [6], along with risk assessment techniques that incorporate statistical models to evaluate the probability and consequences of failure [7].

Complementing these approaches, scaled-model testing has offered valuable data on tunnel performance under stress, such as through small-scale (1:30) model tests [7], shaking table tests where scaled tunnel models were subjected to varying seismic intensities to study the effects of voids [8–11], and experimental investigations conducted to examine the effect of twin voids behind tunnel linings on their progressive failure process [12]. Moreover, computational numerical analyses such as the extended finite element method (XFEM) have been employed to model the development of cracking patterns and distribution in tunnel linings affected by defects such as local cavities and insufficient lining thickness [13,14], and numerical models of tunnels' dynamic responses have been optimized using improved inversion results [15,16]. These studies provide valuable references for preventing and repairing lining cracks influenced by voids behind tunnel linings.

Fiber-reinforced polymer (GFRP) reinforcement and fiber-reinforced concrete (FRC) have also been frequently used in studies on tunnel lining reinforcement [17–19]. In contrast, fiber-reinforced plastic with polymer cement mortar (FRP-PCM) represents an efficacious method for tunnel reinforcement, offering benefits such as ease of application, consistent reinforcement outcomes, lightweight characteristics, and high tensile strength [20]. In this study, we aimed to enhance the sensitivity analysis of the reinforcement method by evaluating the impact of voids through an analysis of bending moments and axial forces within the tunnel lining [21]. In hydraulic structures where moisture and aggressive environmental conditions are prevalent, FRP grids help improve the durability and longevity of the concrete. Proper adhesion ensures that the FRP grid can effectively transfer stress and reinforce the structure. The surface texture and resin properties of FRP grids play significant roles in enhancing this bond. This study involved simulating tunnel linings that had been reinforced with FRP and assessing the effects of such reinforcement in tunnels afflicted with various structural problems. The reinforcement effect of the fiber-reinforced polymer and phase change material (FRP-PCM) method on tunnel lining has been discussed in previous work [22,23]. Namli et al. [24] used fiber reinforcement to construct primary (initial) tunnel linings and secondary (final) tunnel linings of metro projects and conducted an analysis in terms of project duration. Caratelli et al. [25] showed it was possible to replace traditional steel reinforcement with glass-fiber-reinforced polymer (GFRP) cages in precast concrete tunnel segmental lining. Wang et al. [26] analyzed and evaluated the structural safety of the Jiao Xiling Tunnel through determining the influence of voids on the tunnel lining structure. Zhang et al. [27] studied the influence of a void behind a side wall and another void on the stress of tunnel lining under different lateral pressure coefficients. Ye et al. [28] analyzed the existence of voids behind the lining from the perspective of design, construction, and operation and studied the influence law of the position and size of the voids with respect to the structure. In this study, we endeavored to furnish insights into the alterations observed in both rock and liner attributable to the presence of voids between these structures. We present a quantitative discussion on the impacts of such voids on the stress and deformation responses of the liner and surrounding rock formations. As shown in Figures 1 and 2 [29], the formation of voids behind a tunnel can also lead to issues such as insufficient lining thickness and exposure of internal reinforcement. In traditional approaches, sensitivity analyses are often limited by the simplified assumptions made regarding the mechanical properties of materials and the interaction between tunnel lining and voids. Previous studies have shown that FRP reinforcement can improve the tensile capacity of tunnel linings and reduce crack propagation, thus enhancing structural integrity. Despite the extensive use of FRP in tunnel reinforcement, there is limited knowledge on the combined effects of FRP grids and polymer cement mortar (PCM), particularly in the context of void defects in tunnel linings. The long-term behavior of tunnel linings reinforced with FRP-PCM under time-dependent factors, such as creep, has not been fully explored. Most studies do not account for time-dependent degradation or how FRP-PCM systems perform under long-term loading conditions. Current sensitivity analyses lack the precision to capture the full range of structural responses to small changes in void characteristics, leaving gaps in our

understanding of how FRP-PCM reinforcement performs under varying void conditions and sizes.

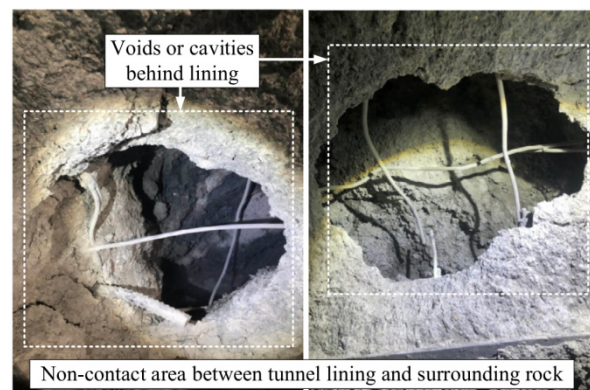


Figure 1. A case of a tunnel lining void problem.

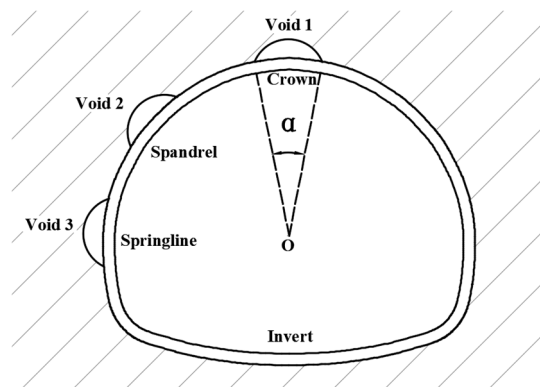


Figure 2. The location of the tunnel void.

In this study, we mainly used the numerical simulation method to carry out the research work on the influence of FRP on structural safety in the case of the investigated tunnel's surrounding rock behind the void. The main stress in the model is the deadweight stress of the soil. The influence of the stress, deformation, and failure of the tunnel under the condition of a void behind the lining was studied. In order to consider the reinforcing effect of FRP, it was compared with the effect of stress, deformation, and failure of the FRP reinforced tunnel. In this study, we improved sensitivity analysis by using different numerical simulation cases that incorporate a more detailed and accurate representation of void variability, FRP-PCM characteristics, and time-dependent effects (creep). This study enhances the precision of sensitivity analysis, leading to more-accurate predictions of the mechanical behavior of tunnel linings and the effectiveness of FRP-PCM reinforcement under varying conditions. The safety factor of the specification is referred to in judging the reinforcement effects of different FRP grades on the tunnel under the influence of time.

Cases of a void behind tunnel lining were considered and then compared after changing the range, position, and number of voids.

2. Research Methods and Evaluation Criteria

2.1. Simulation Methods for Research

(1) Selecting the mechanical model of surrounding rock

The finite element program ABAQUS 2020 was used to establish a plane model. ABAQUS 2020 software is generally applied for simulating the behavior of tunnel lining structure. The cases of voids behind the tunnel lining were considered and then compared after changing the range, position, and number of voids [21,30]. In this study, when we

conducted numerical simulation analysis, the properties of the surrounding rock were determined using an elastic–plastic mechanics model. At present, in the field of geotechnical engineering, people generally choose the ideal elastoplastic model calculation, mainly because (1) the modeling is relatively simple and (2) it allows one to easily obtain numerical simulation parameters using the most common simulation experiments.

In this study, the geological structure method model, also known as the composite integral model, a type of modern rock mechanics calculation model, was used for tunnel structure calculation. This model regards the support structure and surrounding rock as one unit, and the support structure and surrounding rock can simultaneously bear the force. The surrounding rock is the most direct and main force unit, and the function of the support structure is to constrain and control the deformation of the surrounding rock towards the interior of the tunnel. When using the geological structure model for finite element method calculations, the surrounding rock and lining structure are discretized into elements that are only connected to each other at nodes, and the load is shifted to act on the nodes. In order to calculate the stress and displacement fields of the rock and soil medium and the lining structure, interpolation functions are used to consider the boundary conditions of the surrounding rock, and matrix force method or matrix displacement method equations are used to solve the unknowns of the nodes. The tunnel geometries are shown in Figure 3.

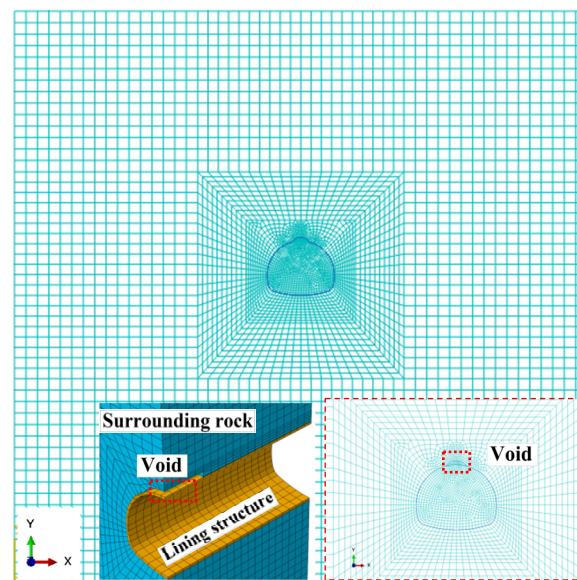


Figure 3. Tunnel geometry in numerical simulations.

(2) Simulating the earth stress field

The biggest advantage of highway tunnels is that they have a large cross-section and a flat shape. As the “long axis” direction of the tunnel structure is horizontal and orthogonal to the direction of the self-weight stress field, the most unfavorable stress field for the structures of highway tunnels is the self-weight stress field. Therefore, this calculation only considers the initial geostress field generated by self-weight.

(3) Determining boundary conditions

The size range of the calculation model and its boundary conditions were selected according to the analytical requirements of tunnel mechanics. Based on engineering practice experience, the impact of underground engineering is “sufficiently small” in areas outside 3–5 times the tunnel diameter from the center of the tunnel. The calculation range of the tunnel model was taken to be four times the tunnel’s diameter of 48 m, so the height and width of the model are both 100 m, and the longitudinal length of the model was taken to be 30 m. The boundary conditions for the computational model are as follows: X direction constraints were applied to the left and right sides of the model in the X direction, no

constraints were applied to the upper boundary in the Y direction, Y direction constraints were applied to the lower boundary in the Y direction, and Z direction constraints were applied to the longitudinal Z direction of the tunnel. The boundary conditions are shown in Figure 4.

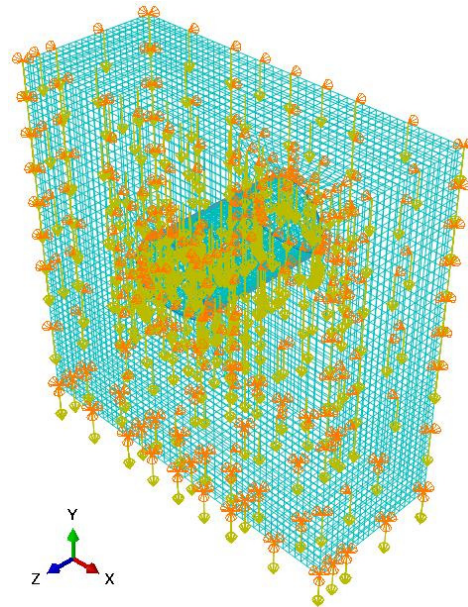


Figure 4. Boundary conditions (Boundary node constraints in orange, and self-weight indicators in yellow).

The height of the void behind the lining was set to 0.45 m, consistent with the thickness of the tunnel lining. The simulation model section was designed as a horseshoe shape, and the radius of the semi-circle is about 9.5 m.

As shown in Table 1, the simulation cases incorporate a more detailed and accurate representation of the following: 1. material behavior—this research models the specific mechanical properties of FRP and PCM, allowing for a more realistic assessment of how these materials interact with the tunnel lining under stress; 2. void variability: by simulating multiple void positions (e.g., crown, spandrel, and springline) and ranges (e.g., 30°, 45°, and 60°), this research offers greater sensitivity to small changes in void characteristics, providing a clearer understanding of their impacts on structural stability; 3. time-dependent effects (creep): the inclusion of creep behavior over time allowed for an assessment of how FRP-PCM reinforcement performs under long-term conditions, a factor that is often neglected in traditional sensitivity analyses.

Table 1. Analysis cases of voids and reinforcement.

Analysis Cases		
Void behind lining	Void range	30°, 45°, 60°
Void behind lining	Void position	Crown, Spandrel, Springline
FRP-PCM reinforcement	Type of FRP grid	FRP-CR4, FRP-CR6, FRP-CR8
FRP-PCM reinforcement	Creep effect	After 5 years, 8 years, 10 years

Tables 2–4 provide mechanical parameters of the different materials involved in tunnel lining reinforcement, including the surrounding rock, tunnel lining, and FRP grid reinforcement. The specific data were sourced from other relevant studies, and using similar values generally does not affect the magnitude of the differences in the simulation results [10,29].

Table 2. Mechanical parameters of the surrounding rock.

Volume Weight of Soil $\gamma/(\text{kN}/\text{m}^3)$	Elastic Modulus E/GPa	Poisson's Ratio μ	Cohesive Force c/kPa	Internal Friction Angle $\varphi/(\text{°})$
20	2.4	0.32	200	30

Table 3. Mechanical parameters of the tunnel lining.

Volume Weight of Soil $\gamma/(\text{kN}/\text{m}^3)$	Elastic Modulus E/GPa	Poisson's Ratio μ	Ultimate Compressive Strength R_a/MPa	Ultimate Tensile Strength R_t/MPa
25	28.0	0.20	19.0	2.0

Table 4. Mechanical parameters of the FRP grid reinforcement material.

		Young's Modulus (MPa)	Compressive Strength (MPa)	Tensile Strength (MPa)	Design Thickness (mm)
FRP Grid	CR4	100,000	-	1400	2.0
	CR6				4.0
	CR8				5.0
PCM		26,000	59.3	4.6	-

2.2. Safety Factors for Evaluating the Stable State of Lining

The basic model based on the actual situation of the void behind the lining is presented in Figure 3. In this study, the influence of the typical patterns of a void behind a tunnel's lining on tunnel deformation was investigated in detail.

According to the JTG D70-2004 Design Specification for Highway Tunnels [31], the ultimate strength of the lining material was used to determine the ultimate bearing capacity N_u of the tunnel structure under eccentric compression. The safety factor, K , of the calculated section was obtained by comparing it with the axial force, N . One can determine whether the safety requirements are met by using Formula (1).

$$K = \frac{N_u}{N} \geq K_s \quad (1)$$

In the formula above, K is the safety factor, N_u is the ultimate bearing capacity of the tunnel structure under eccentric compression, N is the axial force of the tunnel lining under compression, and K_s is the limit value of the safety factor specified in the specifications.

When the axial eccentricity $e_0 \leq 0.20 h$, the ultimate bearing capacity of the compressive strength of the lining structure under eccentric compression of a concrete rectangular section should be calculated according to Equation (2):

$$N_u = \varphi \alpha R_a b h \quad (2)$$

In the formula above, R_a is the compressive ultimate strength of concrete (MPa); b is the width of the lining section (m), taken as 1 m; h is the thickness of the lining section (m), taken according to the actual thickness; φ is the longitudinal bending coefficient of the component, taken as 1 for the tunnel lining; and α is the eccentricity influence coefficient of axial force.

The compressive strength safety factor of the lining structure section was calculated according to Formula (3):

$$K = \frac{N_u}{N} = \frac{\varphi \alpha R_a b h}{N} \quad (3)$$

In this formula, N represents the axial force (kN).

When $e_0 > 0.20 h$, the lining section must be determined based on tensile strength verification. According to the crack resistance requirements, the ultimate bearing capacity of the tensile strength of the lining structure under eccentric compression of a rectangular concrete section should be calculated according to Equation (4).

$$N_u = \frac{1.75R_tbh\varphi}{\frac{6e_0}{h-1}} \tag{4}$$

In the formula above, R_t is the ultimate tensile strength of concrete (MPa).

The safety factor for the tensile strength of the lining structure section was calculated according to Formula (5):

$$K = \frac{N_u}{N} = \frac{1.75R_tbh\varphi}{N\left(\frac{6e_0}{h-1}\right)} \tag{5}$$

The reinforcement mechanism and internal structure of the FRP grid are shown in Figure 5 [22]. Detailed visualizations of FRP grid reinforcement and the setup used for the numerical simulations of tunnel linings with voids are shown. We calculated the axial force, N , and bending moment, M , of the lining structure, and based on the void behind the lining, we used Formulas (3) and (5) to calculate the safety factor of the lining section and compared it with the standard value of the safety factor in the “Design Code for Highway Tunnels”. Based on this specification, the safety state of the tunnel structure under the condition of a void behind the lining was studied.

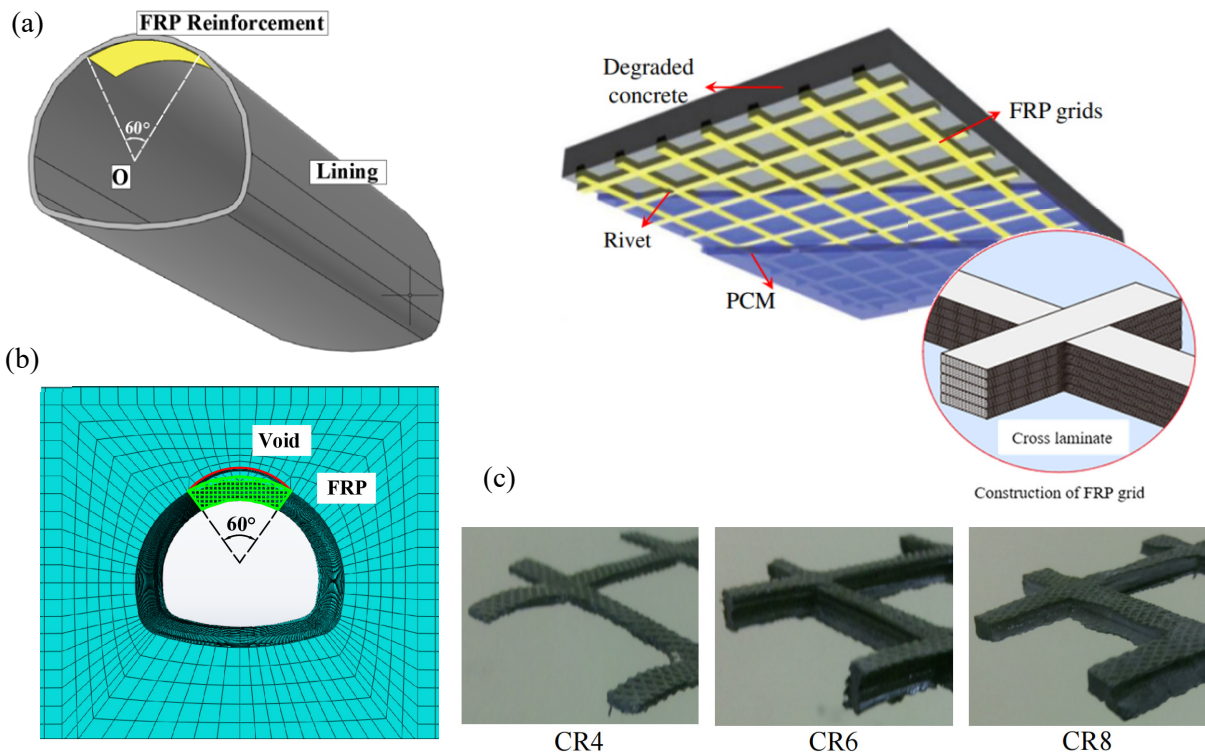


Figure 5. Numerical simulation arrangement and internal structures of the FRP grids. (a) Visualization of the FRP arrangement. (b) Planar numerical simulation layout. (c) Different types of FRP grids.

The distribution of the bending moment and axial force is shown on the left, while the right shows the distribution of the safety factor. The limit value of the safety factor is 2.00. When the safety factor of a certain position is less than the limit value, it is judged as unsafe [31].

In this study, an FRP grid was used as the reinforcing material for the lining area in the unsafe state. CR4 represents a grid thickness of 2 mm. The bending moment and axial

force after reinforcement are shown below. The material for the lining area is in an unsafe state. CR4 represents a grid thickness of 2 mm. The bending moment and axial force after reinforcement are shown below.

3. Results and Analysis

Based on the research results, we planned to study the following principal content.

3.1. The Influence of Void Location and FRP Reinforcement

The material properties of FRP are very different from those of traditional structural materials such as steel and concrete, and their forms are varied. Fiber is the main mechanical material in FRP, and it can be divided into long fiber and short fiber. The reinforcement in the FRP used in engineering structure is mainly long fiber. Continuous fibers can range from several meters to over 100 m in length depending on how they are laid out in the structure (e.g., in unidirectional or woven format). In most applications, such as in structural reinforcements or load-bearing components, fiber lengths are designed to match or exceed the dimensions of the component being reinforced to maximize strength. The long fibers used in FRP reinforcement for engineering structures are generally continuous fibers, which can be several meters long or even much longer, depending on the specific design and application. Apart from the specific strength and specific modulus with respect to the size of the actual engineering result, the material application effect of carbon fiber is the best, but the elongation of carbon fiber material is very low, so it sometimes needs to be mixed with other fibers to achieve better performance. Carbon fiber FRP has become a very important structural reinforcement material, and it has been widely used and developed in the renovation and reinforcement of various civil and industrial buildings.

The FRP-PCM method should be used to ensure the required performance of a repaired or reinforced concrete structure in regard to aspects such as safety, fatigue durability, usability, and environmental impact durability. Therefore, it is necessary to fully investigate and understand the environment in which the existing concrete structure to be repaired or reinforced is situated, along with the damage it has sustained, before construction and implement the measures before and after construction according to the specific needs of the project [31–33].

According to the current research, the void behind the lining was determined to be a common problem, and after analyzing the effect of different void toroidal ranges and locations on the tunnel lining, the distribution characteristics of tunnel lining structure problems were obtained. Based on the specific parameters of tunnel problems in the literature, a tunnel model was established using the numerical simulation method in order to analyze reinforcement behavior.

The effect of reinforcement needed to be considered, and an indicator needed to be introduced to facilitate the comparison of the repair effect and time impact. So, here, we introduce the concept of the sectional repair rate [34].

$$R = \frac{K}{K_0} - 1 \times 100\% \quad (6)$$

In the formula above, R is the sectional repair rate, K represents the safety factor of the lining with FRP reinforcement, and K_0 is the safety factor in the initial state.

The FRP construction example refers to the crack repair work of NEXCO West Japan's lining reinforcement project in the Nagasaki do Hidake Tunnel [35].

The bending moment, axial force, and safety factor were calculated using Formulas (3) and (5).

The stress and strain of the tunnel structure were analyzed by simulating the voids in different positions and ranges behind the lining, and the safety of the structure was evaluated. The evaluation indexes of tunnel lining damage in the current code were sorted out to provide data support for the subsequent research on the effect of a void behind tunnel lining and the evaluation of tunnel lining health. Stress is generally concentrated at

the edge of the void, significantly increasing the compressive force. Concrete structures have much less tensile strength than compressive strength, so the safety factor of such structures is significantly reduced, but reinforcing the lining can effectively improve the soundness in the void range. The bending moment, axial force, and safety factor after reinforcement are shown in Figures 6–10.

According to significant variations in the bending moment values at different locations, the maximum-to-minimum ratio can reach up to fivefold. To facilitate an intuitive statistical comparison, the natural logarithm of the bending moment values was uniformly summarized.

By comparing the effects of voids in different positions in tunnel lining structures, it becomes evident that the safety factor is lower at the center of a void. Notably, the bending moment distribution graph we created reveals tensile forces acting at this location. For concrete structures, the tensile capacity is typically one-tenth of the compressive capacity.

Consequently, when voids occur behind the lining, the safety factor significantly decreases for this structural position. The most pronounced reduction occurs when the void is located at the arch crown, as the stress concentration combines with gravitational effects. This position lies at the tunnel's highest point and along its central axis, preventing the transfer of pressure to other void-free areas.

Figure 6 shows the displacement (U2) contours of a tunnel lining under deformation, both without FRP reinforcement and with three different types of FRP reinforcement: CR4, CR6, and CR8. The color scale represents the magnitude of displacement. In contrast to bending moments, the axial force variations do not exhibit specific characteristics related to void positions. Instead, they uniformly increase after the development of a void. Since safety factors are calculated based on both bending moments and axial forces, only axial force changes for void-free and arch crown void scenarios are presented. The most significant improvement was observed with the CR8 reinforcement. The displacement across the tunnel lining was more uniform, with only a small amount of orange and yellow at the bottom. The maximum displacement was reduced to $+3.323 \times 10^{-3}$, representing the strongest performance among the reinforcement types. The bottom of the tunnel lining experienced the greatest displacement in all cases, but this was significantly mitigated with FRP reinforcement. CR8 provided the most effective reduction in displacement.

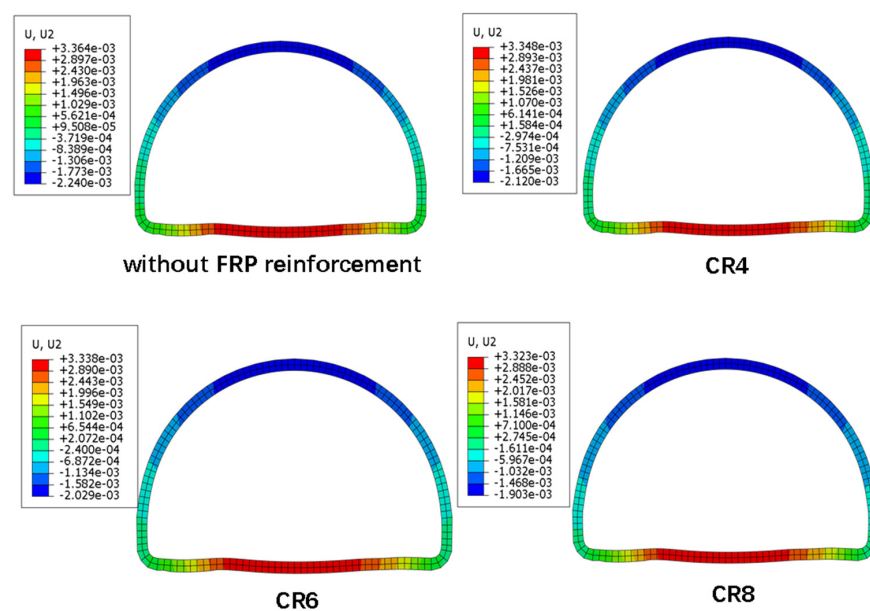


Figure 6. The deformation analysis of the lining structure.

Figure 7 shows the distribution of internal forces in the tunnel lining under different void ranges, where the void range gradually expands from 30 degrees to 60 degrees. Based

on actual tunnel conditions, voids larger than 60 degrees are rarely encountered. During the expansion of a void, the change in bending moment is particularly noticeable. The bending moment at the top of the tunnel transitions from compressive to tensile, and the rate of increase in the tensile bending moment is higher than the rate of increase in the void range. Since the bending moment values have different directions, and there is a large difference between the maximum and minimum values, the bending moment values shown in this diagram are the natural logarithms of the values. The range of $\ln(-190 \text{ to } 190)$ is from -6 to 6 . Additionally, as the void range increases, the area affected by the tensile bending moment also increases. Given that the tensile strength of concrete is much lower than its compressive strength, assessing the safety factor becomes particularly important. The safety factor analysis could be achieved through an analysis of Figure 7c, showing that the safety factor at the center of the void decreased most significantly, and the rate of decrease could be calculated. The rates of decrease or increase in the safety factor for every one-degree expansion of the void are as follows:

- In the range of 0–30 degrees, the rate of decrease in the tensile bending moment is 16.67%;
- In the range of 30–45 degrees, the rate of increase is 20%;
- In the range of 45–60 degrees, the rate of decrease is 56.67%.

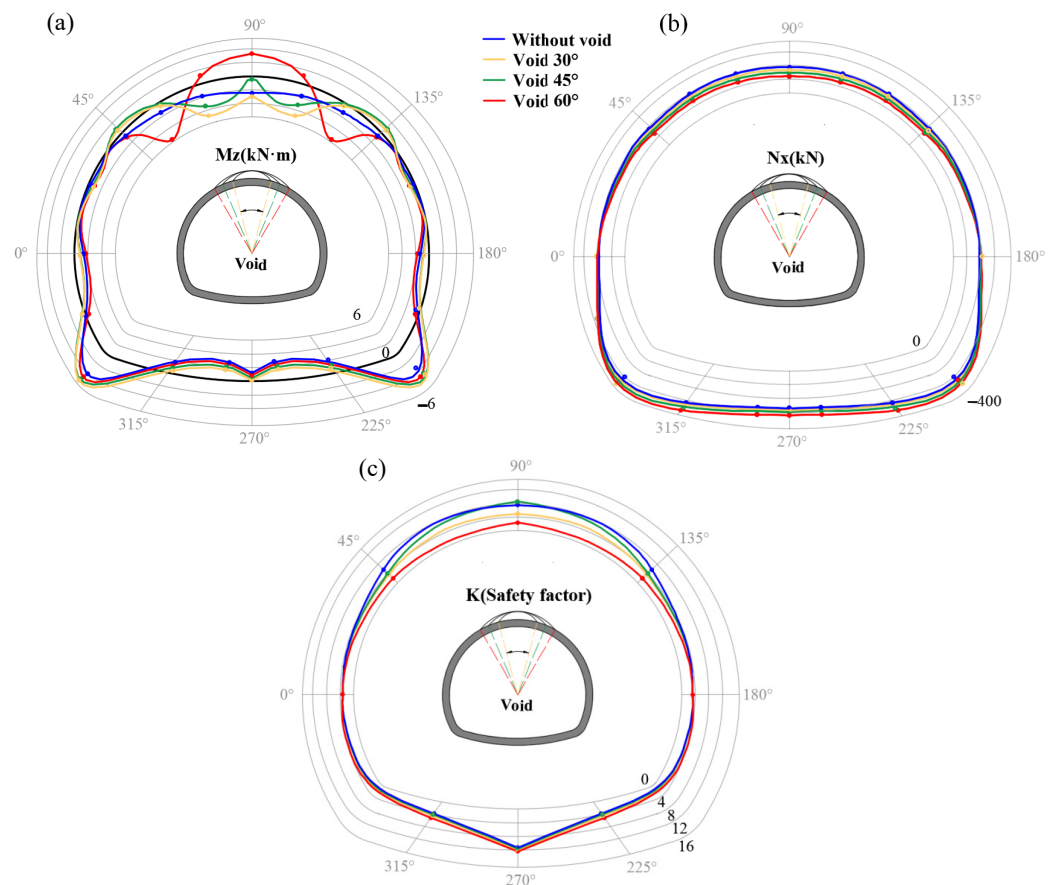


Figure 7. The inner force of the tunnel with different void ranges: (a) bending moment; (b) axial force; (c) safety factor.

The axial force change presents a linear trend. With the expansion in the void range at the top, the overall axial force on the tunnel lining decreases, the axial force on the top and shoulder decreases significantly, and there is a sudden change in axial force between the shoulder and the waist. Moreover, the internal force adjustment of the lining brought about by stress redistribution causes the load in the shoulder area to transfer to the waist, so the axial force suddenly increases in the waist position.

Regarding the bending moment trend, when the void range is small (30°), the bending moment at the center of the void is positive because the lining is under pressure from the transformation of the weight of the overlying soil. At this time, the soil load slightly increases compared with that in the condition without a void because there is an obvious stress concentration phenomenon on both sides of the void, and the center of the void is relatively close to the stress concentration point, so the bending moment increases, and the safety factor decreases compared with the condition without void; that is, the safety of the lining decreases.

Figures 8 and 9 display the bending moment (Mz) and axial force (Nx) distribution around the tunnel lining under different conditions. These diagrams show how voids and FRP reinforcement influence the internal forces acting on the tunnel lining. When the void range is large (60°), the soil load within the void range can no longer be transferred, so the load size is 0. At this point, the force on both sides of the void and lining shoulder generates a bending moment at the center of the void, and the bending moment is negative. It is subject to great tensile force because the tensile performance of concrete is poor, amounting to approximately one tenth of its compressive strength. Therefore, in the case of a large void, the lining safety factor is much lower and close to the limit value; thus, the corresponding safety factor is so poor that the lining can be very easily damaged.

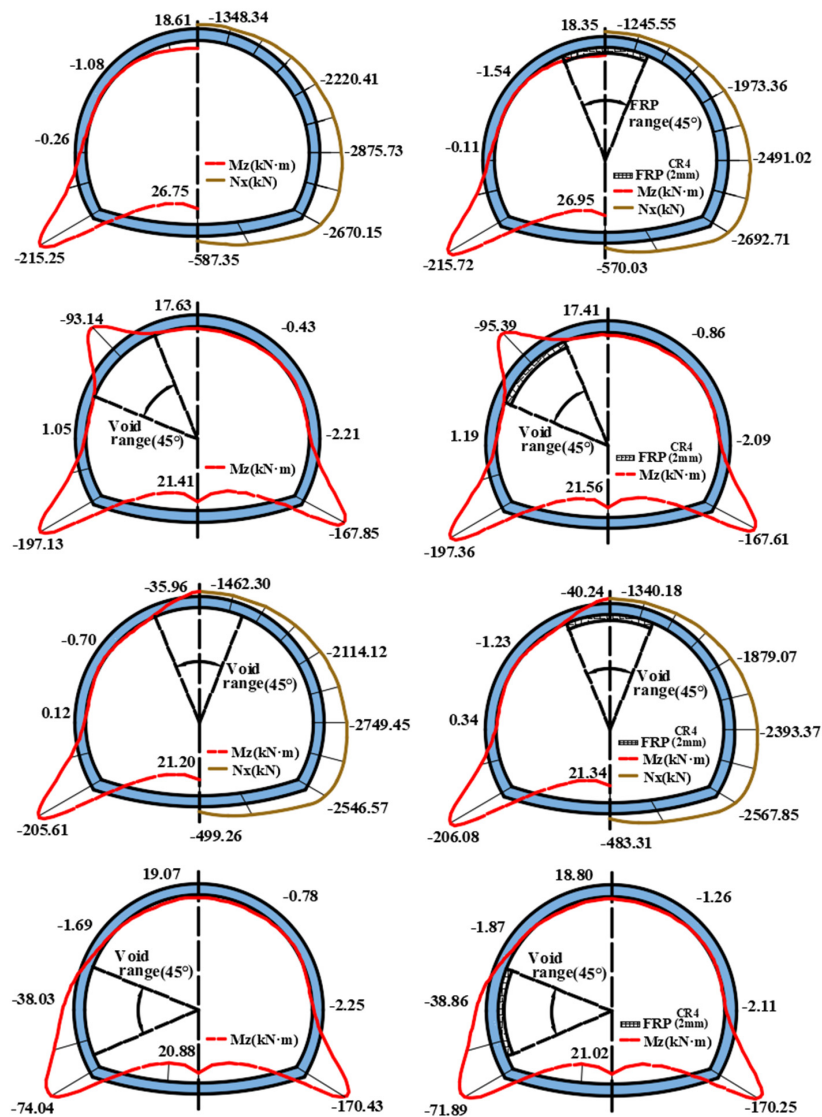


Figure 8. Bending moment and safety factory.

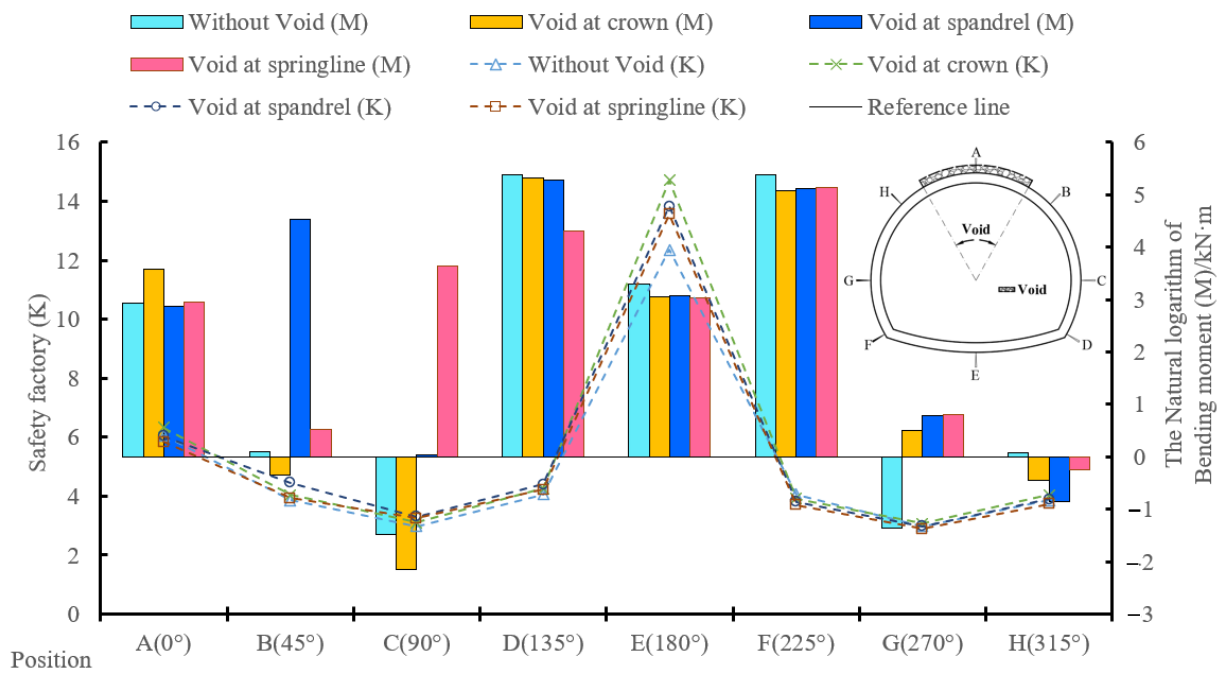


Figure 9. Bending moment and safety factor.

In Figure 9, we can observe the impacts of different void positions on the internal forces of the tunnel lining. When the void range is 45 degrees, the bending moment at the center of the void significantly increases in the tensile direction, with the tensile increase at the shoulder void being the most prominent.

Table 5 and Figure 10 shows the distribution of the safety factor and bending moment at different void locations. Using eight symmetrically arranged monitoring points along the cross-section of the tunnel lining, we can see the distribution of internal forces, with point A at the top of the tunnel serving as the center of symmetry. The bar graph represents the bending moment distribution, wherein the vertical axis on the right shows positive and negative values, while the line graph represents the safety factor, with its vertical axis on the left showing only positive values. The safety factor limit was set at 2.0, indicating that monitoring points where the safety factor approaches 2 are more prone to structural imbalance or imminent failure. The safety factor at point E of the inverted arch remained consistently high due to its lower position, where gravitational influence is minimal, and it is under vehicle load in actual operation. Therefore, its static structural stability is not the focus of this study. By comparing the safety factors at points A, B, and C under three different void conditions, it is evident that the safety factor decreases most significantly at the monitoring point located at the center of the void.

Table 5. Repair rate of safety factor with FRP reinforcement.

Position	Repair Rate of Safety Factor (%)			
	Void at Crown (45°)	FRP-PCM (CR4)	FRP-PCM (CR6)	FRP-PCM (CR8)
Crown (0°)	6.05	14.84%	27.90%	56.89%
Spandrel (45°)	3.86	12.63%	25.59%	52.85%
Springline (90°)	2.97	10.94%	23.11%	46.07%
Bottom of side wall (135°)	4.06	−0.95%	−1.61%	−2.33%
Invert (180°)	12.35	2.62%	5.22%	10.30%

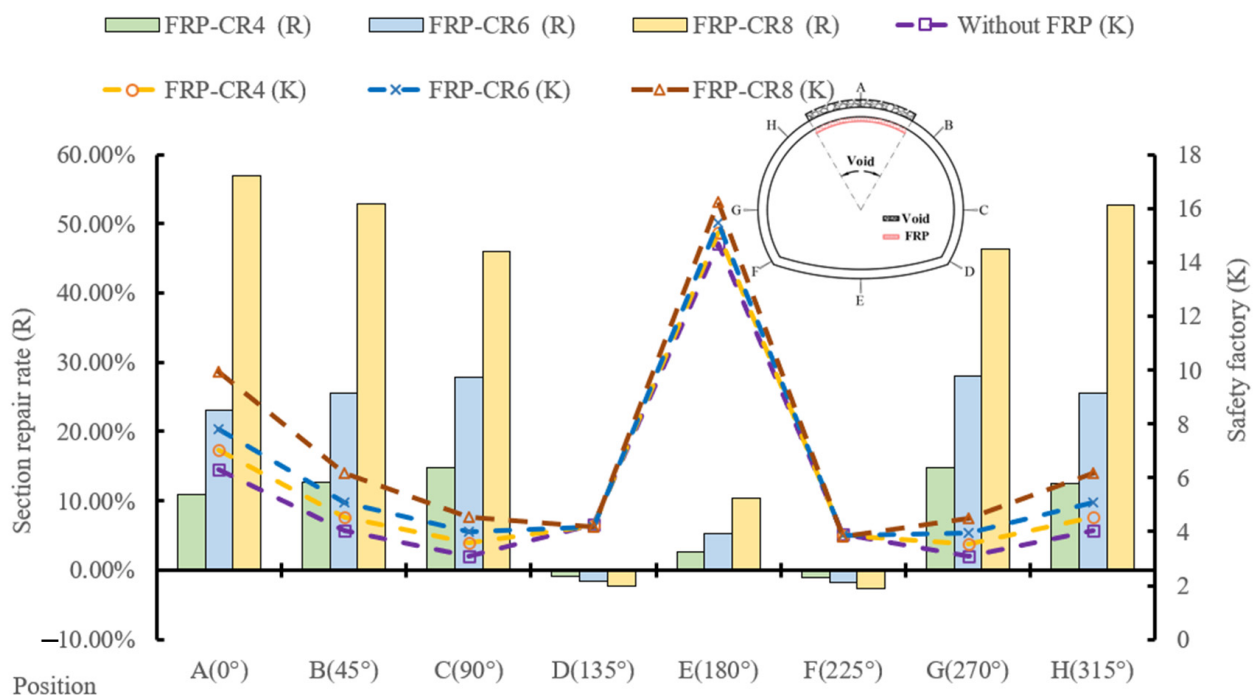


Figure 10. The safety factor and section repair rate with FRP reinforcement.

Furthermore, beyond considering internal force changes due to voids at different positions, it is essential to investigate the impact of FRP-PCM reinforcement. Figure 10 compares the reinforcement effects of different types of FRP grids when the top void range is 45 degrees. As shown in Figure 9, the analysis was conducted by comparing the bending moment and safety factor. These two cases exhibit symmetry. Overall, axial forces do not produce isolated tensile or compressive variations due to the presence of a void; the magnitude changes uniformly.

After each set of scenarios, reinforcement studies were conducted. Due to the extensive data, the internal force distribution graph includes CR4-grade FRP grids as post-reinforcement cases. Detailed reinforcement comparisons are available in tabular form, including analyses of CR6 and CR8 reinforcement effects. Overall, the pre- and post-reinforcement internal force distributions of the lining exhibit consistency, but specific numerical differences are evident. For evaluation purposes, the safety factor was employed directly. Comparing it with the cross-sectional repair rate revealed that larger FRP grid models enhance lining safety and repair effectiveness.

Notably, the repair rate is highest at the centers of the voids, approaching 60%. Furthermore, comparing the safety factor for the void-free condition shows that the efficacy of CR8-type reinforcement surpasses that of the lining in an undamaged state. Additionally, the influence range of reinforcement decreases with increasing distance, aligning with general trends. When voids are of moderate or smaller size, partial reinforcement at specific positions is feasible, reducing economic costs. Finally, the safety factor at the position of the crown is exceptionally high, and due to its distance from voids and reinforcement centers, the variation is minimal. However, the crown's position falls within the load-bearing zone. Through the above two parameters, bending moment and axial force, the change in safety factor could be calculated.

Regarding void location, a void located at the spandrel is more dangerous than a void at the crown, especially for the cross range between the crown and the void, and there are severe tension and stress concentration phenomena. According to the simulation results, the safety factor is lower than the standard limit value, and it is very easy for damage to occur. Finally, when the number of voids increases, the safety factor does not linearly

decrease but reaches a delicate balance. The influence of multiple voids can be further discussed in future studies.

3.2. The Influence of the Creep Phenomenon

Creep is an important form of material flow deformation. By observing the deformation behaviors of many materials under tensile load, it can be found that under a constant temperature and constant load, the deformation of specimens will slowly increase with the increase in time, a process called the creep phenomenon. This is a narrow definition [36]. The creep analysis mode of Abaqus software usually uses three creep laws to describe the behavior of visco-plastic materials. The power law model can be applied to simulate creep behavior under isothermal and fixed loads, and the laws used are the time-hardening rate and strain-hardening rate relationship equations. To determine the goodness of the fit between creep parameters and reference experimental data curves (a mathematical analysis method used to obtain material parameters), the coefficient of determination R (R square) of regression analysis is used as the basis for judgment. The R value ranges from 0 to 1, and the closer R is to 1, the better the fitting result [37]. To simplify the calculation of creep problems in plastic structures (such as reducing the coupling between creep strain and other inelastic strains), the analysis can be divided into a static loading process and a subsequent analysis of the creep process. The static loading process is a time-independent loading process.

3.2.1. Calculation of the Creep Process

After the static analysis in step 1, a stress field was generated within the structure, and the calculation of the parameters of the creep process could proceed. The creep calculation was mainly divided into two parts: obtaining the creep model parameters of the material and setting up the creep analysis step.

(1) Obtaining the Material Creep Model Parameters

Currently, Abaqus provides three types of creep models: the power-law model and the hyperbolic sine law model. The power-law model has two forms: the time-hardening form and the strain-hardening form. The time-hardening form is the simplest, and it is particularly suitable for simple creep processes (such as those where the stress variation is not significant during the creep process). Its differential form is given in Equation (7).

The equation shown in the image is the differential form of the time-hardening form of the power-law model for creep:

$$\dot{\varepsilon}^{cr} = A(q^*)^n t^m \quad (7)$$

The variables in the above equation are defined below.

$\dot{\varepsilon}^{cr}$ is the equivalent creep strain rate.

q^* is the equivalent deviatoric stress.

t is time.

A , n , and m are constants, representing the material's creep properties.

This equation is used to describe the creep behavior of materials, with constants A , n , and m being determined experimentally for a given material. The equivalent creep strain rate is dependent on both the equivalent deviatoric stress and time.

Figure 11 represents the relationship between creep strain, time, and equivalent stress, for which Equation (7) must be integrated. The result of the integration is shown in Equation (8):

$$\varepsilon^{cr} = \frac{A}{m+1} (q^*)^n t^{m+1} \quad (8)$$

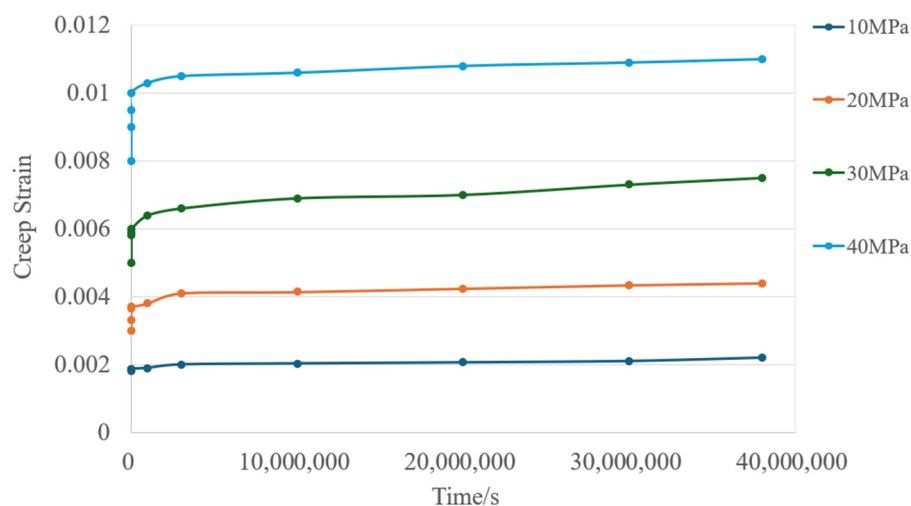


Figure 11. Creep time curve (Under different stress conditions).

This integrated form of the equation gives the total creep strain $\dot{\epsilon}^{cr}$ as a function of time t , the equivalent deviatoric stress q^* , and the material constants A , n , and m . It describes how the creep strain accumulates over time under a constant equivalent stress.

In Figure 11, the x -axis represents time in seconds, and the graph spans up to around 40 million seconds, or approximately 463 days. Over this period, the creep strain increased significantly at higher stress levels, while the lower stress levels show relatively minimal increases. This behavior is crucial when considering the long-term performance of materials in structural applications, such as tunnel linings, where sustained loads and time-dependent deformation must be carefully accounted for to ensure stability over extended periods.

3.2.2. Creep Calculation

Since creep is a time-dependent process, it is crucial to explicitly consider time in the analysis. Creep develops gradually under a sustained load, and its effects become more pronounced as time progresses, influencing the long-term performance and stability of materials. However, unlike dynamic processes, creep is characterized by slow deformation over time rather than rapid changes, meaning that inertia effects, such as those associated with the acceleration of the structure, are negligible [37]. This fact simplifies the analysis because the forces resulting from changes in velocity or acceleration do not need to be considered. Instead, the focus is on the gradual strain accumulation due to constant stress over an extended period, making it a quasi-static problem. By understanding and accounting for this, the long-term safety and serviceability of structures can be accurately assessed without the complexities of dynamic analysis. To handle these characteristics, ABAQUS provides specific analysis steps designed for this type of process.

Constitutive model identification includes the determination of the model's structure and parameters, the principle for which is derived from control theory. Selecting an appropriate creep model and determining the corresponding parameters constitute an important part of creep research. The safety performance of a tunnel must be judged not only by the stress condition after excavation but also by the stress condition of the tunnel under the influence of time factors.

In fact, as the deformation of a material increases with time, its stress also changes. Therefore, creep broadly refers to change of the stress and deformation under the action of a constant external force over time. The characteristic of this phenomenon is that deformation, stress, and external force no longer maintain a one-to-one correspondence relationship; even when the stress is less than the yield limit, the deformation still has the property of irreversible deformation. We conducted a deformation analysis of the lining structure. In order to fully grasp the FRP-PCM reinforcing performance of the lining structure, the figure below shows the vertical safety factor of the lining structure under the influence of creep

action on the lining void. As can be seen from the figure, the deformation of the lining structure progressively decreases with the increase in FRP-PCM grade at the reinforcing and strengthening parts.

Due to the relatively small values of creep strain, the change in the safety factor over a 10-year period was selected as the main focus of analysis in this study. Based on the calculation examples of three different reinforcement types, void positions, and creep times, the decrease in the safety factor was taken as the focus of the analysis.

In reference to Figure 12, by comparing the effects over time, it can be observed that as the reinforcement model improves, the impact of creep on reinforcement diminishes. Simultaneously, the reinforcement is influenced by gravity. At the crown of the arch, the creep effect is most pronounced, while at the springline, the height is lower. Additionally, the direction of the reinforcement support force differs from that at the crown, resulting in a reduced time-dependent impact on reinforcement at the springline.

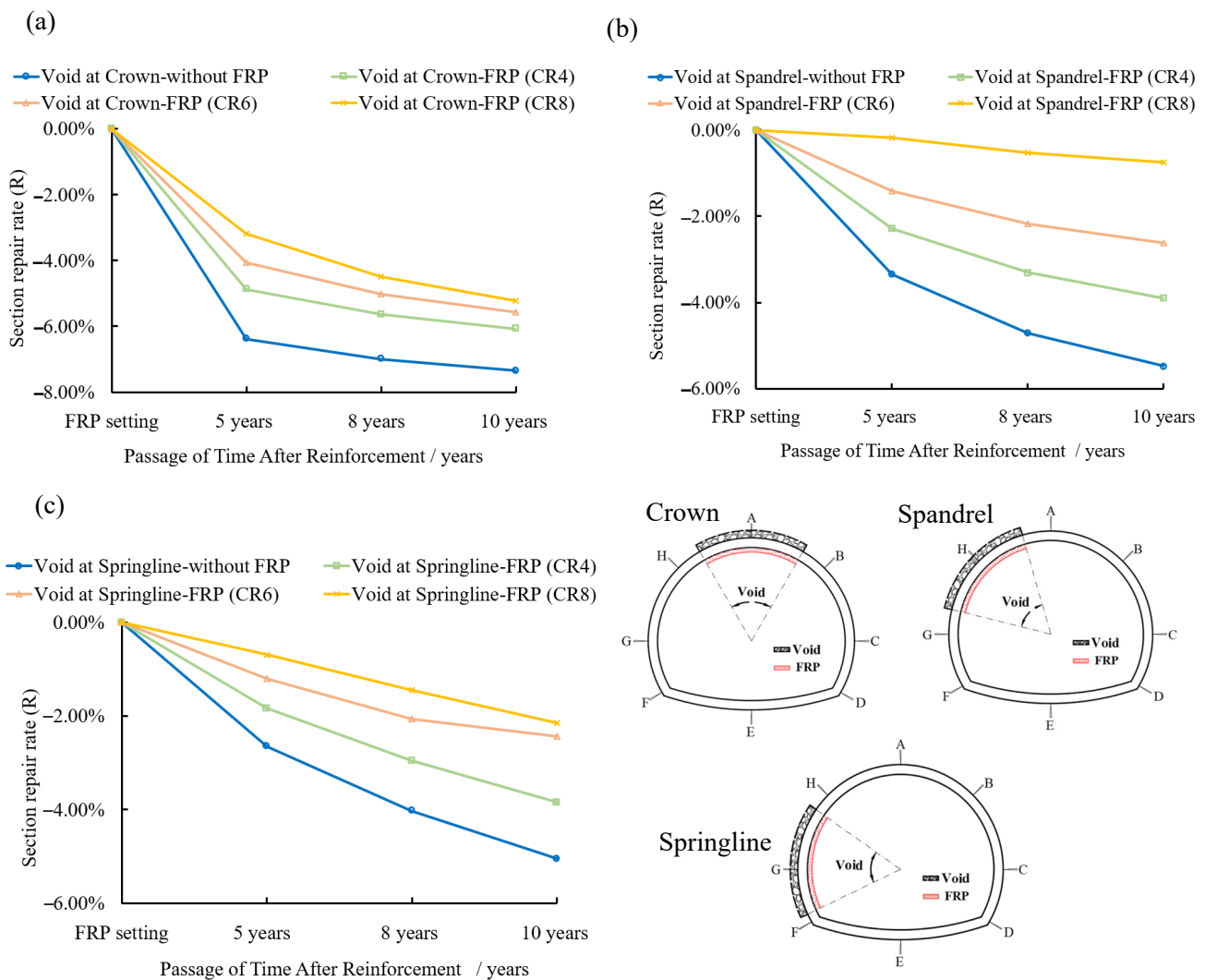


Figure 12. The section repair rates of different void positions under the creep effect: (a) void at the crown; (b) void at the spandrel; (c) void at the springline.

Furthermore, even at the crown, where the creep effect is most evident, the maximum deterioration rate does not exceed 8%. After reinforcement, the safety factor significantly improves. Compared to the section repair rate of 40–60%, creep causes only an 8% deterioration over an extended period when the reinforcement is effective, and this value is acceptable. In reference to Figure 13, for the case “Void at Crown”, without FRP, the safety factor declines significantly, reaching a 7.35% decrease after 10 years. FRP reinforcement

improves the situation, with CR8 showing the best performance, reducing the safety factor decline to 5.22% after 10 years, which can be compared to 6.07% for CR4. Over time, FRP effectively mitigates the reduction in safety factors, with the higher-grade FRP (CR8) being more effective.

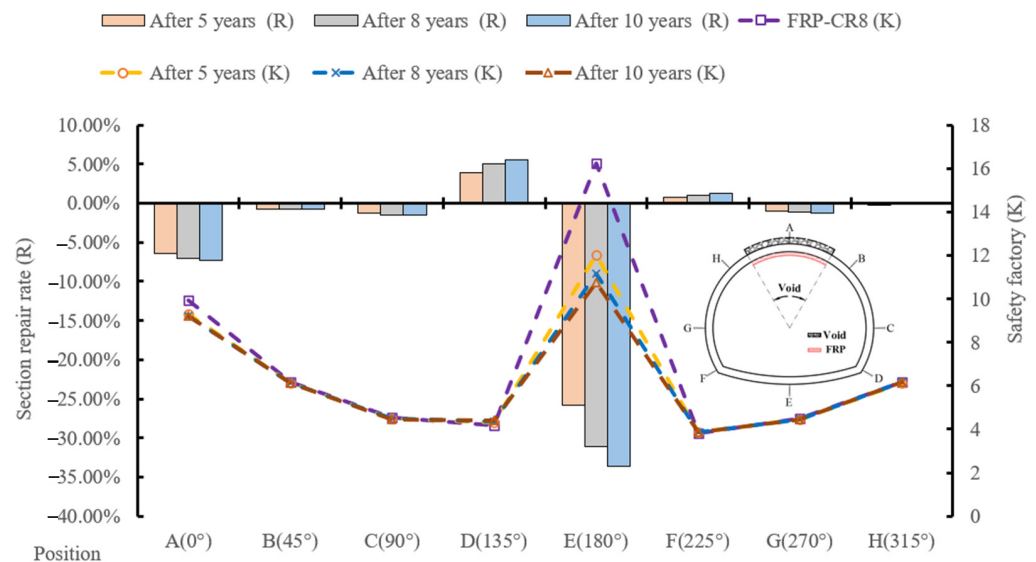


Figure 13. The safety factor and section repair rate with creep effects.

As shown in Figure 13, after 5, 8, and 10 years, the section repair rates at different positions show how effective the reinforcement is in repairing or stabilizing the tunnel lining over time. The largest section repair rate improvements can be observed at position E (180°), indicating that this area, typically the invert or bottom of the tunnel, experiences the greatest benefit from reinforcement measures. In contrast, positions such as A (0°), B (45°), and F (225°) show negative section repair rates, meaning that these areas either continue to deteriorate or did not significantly benefit from reinforcement over the time period. The results show that the CR8 FRP consistently performs the best, reducing the decline in safety factors more effectively compared to CR4 and CR6. Additionally, the spandrel position shows the most significant improvement when reinforced with FRP, while the crown and springline positions still experience moderate declines in safety factors over time, despite FRP reinforcement. When lining is built without FRP reinforcement, the safety factor declines are considerably worse in all locations, indicating the critical importance of FRP reinforcement for long-term tunnel stability. FRP grids, especially CR8, play a crucial role in maintaining tunnel stability over time. The spandrel position benefits the most from FRP reinforcement, while the crown and springline positions still experience safety factor decreases, albeit less than in cases without reinforcement. The data suggest that the higher-grade FRP (CR8) is the most effective at mitigating the reduction in safety factors, particularly over longer time frames.

3.3. The Key Research Findings

From the comparison of the displacement results over different periods and safety factors, it can be observed that the surrounding rock undergoes overall movement after construction, with particularly significant changes at the construction site. This occurs because, after construction, the surrounding rock loses its external constraints, causing it to shift inward, and this movement also pulls in deeper rock masses, reflecting the spatial effects generated during the construction process. However, as time progresses, the displacement values gradually decrease, indicating that the tunnel is approaching stability and entering a new equilibrium state. Upon comparing the results at different stages, it is evident that the reinforcement effect of FRP is significant, especially in areas where the lining is relatively weak, such as the arch crown or regions near hollow defects, where the

safety factor is lower. Over time, the stress state of the surrounding rock tends to stabilize, and changes in the lining's safety factor become smaller. FRP played a positive role in reinforcing the lining at various cavities across different periods, contributing to the overall stability of the structure. In this study, we captured the full range of structural responses to small changes in void characteristics and how FRP-PCM reinforcement performs under varying void conditions and sizes.

4. Conclusions

In this study, numerical simulation methods were used to compare the existence of different voids and repair effects, and the safety factor was used as a safety evaluation index to provide ideas on improving design around the void behind a tunnel.

Different void positions (such as at the crown, spandrel, and springline) and their impacts on the tunnel lining's mechanical behavior were analyzed. The simulation results show that voids at the crown (top) are particularly critical, leading to higher stress concentrations and a greater need for reinforcement.

This study demonstrates that FRP-PCM reinforcement significantly improves the mechanical behavior of tunnel linings. The following safety factor improvements were noted: The safety factor increased significantly after reinforcement, especially when higher-grade FRP grids such as CR8 were used. In some cases, the safety factor even surpassed that in the pre-void condition, indicating that FRP-PCM can restore and exceed the original structural integrity. FRP provides high tensile strength, significantly reinforcing areas prone to stress, such as the arch crown, sidewalls, and regions with existing defects (e.g., hollow areas). This reinforcement helps distribute loads more evenly and reduces the likelihood of structural failure or large deformations. PCM, on the other hand, improves the compressive strength and adhesion of the lining, especially in areas where traditional materials might crack or deteriorate over time. The time-dependent deformation (creep) of tunnel lining is an essential factor in assessing the long-term effectiveness of FRP-PCM. Over a period of 5 to 10 years, the simulations show that FRP-PCM significantly mitigates the negative effects of creep, ensuring the tunnel lining remains structurally sound over extended periods. Over time, the stress state in the surrounding rock stabilizes as the construction-induced displacements reduce in severity. FRP-PCM reinforcement plays a crucial role in helping the tunnel lining maintain its shape and structural integrity during this stabilization phase. As shown in the displacement results, the tunnel moves toward a stable equilibrium faster when reinforced with FRP-PCM, reducing long-term maintenance needs.

To prevent future issues, a combination of regular monitoring, proactive maintenance, effective drainage, and localized strengthening should be adopted to ensure the ongoing safety and durability of tunnel structures reinforced with FRP-PCM.

Author Contributions: Data curation, Q.L.; formal analysis, Q.L.; methodology, Y.J.; resources, Y.J. and S.S.; software, J.W.; writing—original draft, Q.L. All authors have read and agreed to the published version of the manuscript.

Funding: This work was supported by JST SPRING, Japan, under grant number JPMJSP2172.

Institutional Review Board Statement: Not applicable.

Informed Consent Statement: Not applicable.

Data Availability Statement: The data presented in this study are available on request from the corresponding author. The data are not publicly available due to the laboratory's privacy restrictions.

Conflicts of Interest: Author Jing Wang was employed by the company MCC Wukan Engineering Technology Co., Ltd. The remaining authors declare that the research was conducted in the absence of any commercial or financial relationships that could be construed as a potential conflict of interest.

References

1. Japan Road Association. *Management Manual of Road Tunnel Maintenance*; Japan Road Association: Tokyo, Japan, 2015; pp. 248–249.
2. Li, J.J.; Fang, Y.; Liu, C.; Zhang, Y.X.; Lu, W.H. Performance investigation of tunnel lining with voids around surrounding rocks. *Adv. Civ. Eng.* **2020**, *3*, 1364984. [[CrossRef](#)]
3. Kusaka, A.; Kishida, N.K.; Isago, N.; Kawata, K. Effect of stiffness of back-fill grouting material against void above tunnel lining upon load-bearing capacity for lining fracture. *J. Tunn. Eng.* **2016**, I-19.
4. Fraldi, M.; Guarracino, F. Limit analysis of collapse mechanisms in voids and tunnels according to the Hoek–Brown failure criterion. *Int. J. Rock Mech. Min.* **2009**, *46*, 665–673. [[CrossRef](#)]
5. Yasuda, N.; Tsukada, K.; Asakura, T. Three-dimensional seismic response of a cylindrical tunnel with voids behind the lining. *Tunn. Undergr. Space Technol.* **2019**, *84*, 399–412. [[CrossRef](#)]
6. Gao, Y.; Jiang, Y.J.; Li, B. Voids delineation behind tunnel lining based on the vibration intensity of microtremors. *Tunn. Undergr. Space Technol.* **2016**, *51*, 338–345. [[CrossRef](#)]
7. Yang, P. Risk Assessment on the Defects behind Lining of Road Tunnels. *China Saf. Sci. J.* **2011**, *21*, 130–135.
8. He, B.G.; Liu, E.R.; Zhang, Z.Q.; Zhang, Y. Failure modes of highway tunnel with voids behind the lining roof. *Tunn. Undergr. Space Technol.* **2021**, *117*, 104147. [[CrossRef](#)]
9. Xin, C.L.; Wang, Z.Z.; Gao, B. Shaking table tests on seismic response and damage mode of tunnel linings in diverse tunnel-void interaction states. *Tunn. Undergr. Space Technol.* **2018**, *77*, 295–304. [[CrossRef](#)]
10. Zi, H.; Ding, Z.; Ji, X.; Liu, Z.; Shi, C. Effect of voids on the seismic vulnerability of mountain tunnels. *Soil Dyn. Earthq. Eng.* **2021**, *148*, 106833. [[CrossRef](#)]
11. Nie, Z.Y.; Zhang, C.L.; Li, F.X. Effect of void behind lining on seismic performance of tunnel. *China Earthq. Eng.* **2015**, *37*, 138–143.
12. Wang, B.; Li, T.B.; He, C.; She, J. Model Test of Effect of Lining Thinning on Tunnel Structure Bearing Capacity. *J. China Railw. Sci.* **2013**, *35*, 106–114.
13. Zhang, X.; Zhang, C.P.; Feng, G.; Han, K.H. Experimental studies on effect of voids behind tunnel linings on progressive failure process of tunnel structures. *Chin. J. Geotech. Eng.* **2017**, *39*, 1137–1144.
14. Ye, Z.J.; Yang, Y.Y.; Ye, Y. Three-dimensional effects of multiple voids behind lining on the mechanical behavior of tunnel structure. *Ain Shams Eng. J.* **2023**, *14*, 101949, ISSN 2090-4479.
15. Fu, J.Y.; Xie, J.W.; Wang, S.Y.; Yang, J.S.; Yang, F.; Pu, H. Cracking Performance of an Operational Tunnel Lining Due to Local Construction Defects. *Int. J. Geomech.* **2019**, *19*, 04019019. [[CrossRef](#)]
16. Meguid, M.A.; Dang, H.K. The effect of erosion voids on existing tunnel linings. *Tunn. Undergr. Space Technol.* **2009**, *24*, 278–286. [[CrossRef](#)]
17. Wu, X.; Bao, X.; Shen, J.; Chen, X.; Cui, H. Evaluation of void defects behind tunnel lining through GPR forward simulation. *Sensors* **2022**, *22*, 9702. [[CrossRef](#)]
18. Hosseini, S.M.; Mousa, S.; Mohamed, H.M.; Ferrier, E.; Benmokrane, B. Experimental and analytical investigation of precast fiber-reinforced concrete (FRC) tunnel lining segments reinforced with glass-FRP bars. *Tunn. Undergr. Space Technol.* **2023**, *139*, 105230. [[CrossRef](#)]
19. De la Fuente, A.; Blanco, A.; Armengou, J.B.; Aguado, A. Sustainability based-approach to determine the concrete type and reinforcement configuration of TBM tunnels linings. Case study: Extension line to Barcelona Airport T1. *Tunn. Undergr. Space Technol.* **2017**, *61*, 179–188. [[CrossRef](#)]
20. Tiberti, G.; Minelli, F.; Plizzari, G. Reinforcement optimization of fiber reinforced concrete linings for conventional tunnels. *Compos. Part B Eng.* **2014**, *58*, 199–207. [[CrossRef](#)]
21. Lin, Q.W.; Han, W.; Jiang, Y.J.; Koga, D. A Study on the Frame Structure Analysis for Lining Design of Existing Tunnel. In Proceedings of the 32nd Tunnel Conference of the Japan Society of Civil Engineers, Tokyo, Japan, November 2022.
22. Jiang, Y.J.; Wang, X.S.; Li, B.; Higashi, Y.; Taniguchi, K.; Ishida, K. Estimation of reinforcing effects of FRP-PCM method on degraded tunnel linings. *Soils Found.* **2017**, *57*, 327–340. [[CrossRef](#)]
23. Hara, T. Corrugate fiber reinforced plastic sheet in repairing tunnel linings. *J. Civ. Eng. Archit.* **2015**, *9*, 684–690.
24. Namli, M. Evaluation of the effect of using fiber reinforcement in tunnel linings for metro projects. *Undergr. Space* **2021**, *6*, 732–750. [[CrossRef](#)]
25. Caratelli, A.; Meda, A.; Rinaldi, Z.; Spagnuolo, S.; Maddaluno, G. Optimization of GFRP reinforcement in precast segments for metro tunnel lining. *Compos. Struct.* **2017**, *181*, 336–346. [[CrossRef](#)]
26. Wang, C.J.; Lei, M.F.; Peng, L.M. Safety Evaluation Model and Method of Tunnel Disease Structure. *J. Railw. Sci. Eng.* **2011**, *8*, 74–77.
27. Zhang, S.L.; Qi, X.Q.; Liu, C.; Chen, D.G. Distribution characteristic of voids behind the lining of highway tunnel and its influence on lining structure. *J. Archit. Civ. Eng.* **2020**, *37*, 62–70.
28. Ye, Z.J.; Ye, Y. Comparison of Detection Effect of Voids Behind Shield Tunnel Segment Using Transient Electromagnetic Radar and Ground Penetration Radar. *Geotech. Geol. Eng.* **2019**, *37*, 4391–4403. [[CrossRef](#)]
29. Wang, J.F.; Huang, H.W.; Xie, X.Y.; Bobet, A. Void-induced liner deformation and stress redistribution. *Tunn. Undergr. Space Technol.* **2014**, *40*, 263–276. [[CrossRef](#)]
30. Hu, J.; Li, S.C.; Liu, H.L.; Li, L.P.; Shi, S.S.; Qin, C.S. New Modified Model for Estimating the Peak Shear Strength of Rock Mass Containing Nonconsecutive Joint Based on a Simulated Experiment. *Int. J. Geomech.* **2020**, *20*, 04020091. [[CrossRef](#)]

31. Ministry of Transportation of the People's Republic of China. *Code for Highway Tunnel Design*; Ministry of Transportation of the People's Republic of China: Beijing, China, 2016.
32. Li, B.; Lei, M.F.; Li, W.H. Safety Influence of Operating Highway Tunnel Caused by Structure Disease. *J. Railw. Sci. Eng.* **2011**, *8*, 40–45.
33. Hollaway, L.C. A review of the present and future utilisation of FRP composites in the civil infrastructure with reference to their important in-service properties. *Constr. Build. Mater.* **2010**, *24*, 2419–2445. [[CrossRef](#)]
34. Yao, J.; Teng, J.G.; Chen, J.F. Experimental study on FRP-to-concrete bonded joints. *Soils Found.* **2017**, *57*, 327–340. [[CrossRef](#)]
35. Nexco West Japan. Nexco Builds Construction Work at Nagasaki Dohgatake Tunnel. 2017. Available online: <https://www.kozobutsu-hozen-journal.net/walks/11455> (accessed on 31 October 2017).
36. Jiang, Y.J.; Zhang, X.P. Evaluation of reinforcement effect of FRP-PCM method in tunnel lining. *Hazard Control Tunn. Undergr. Eng.* **2020**, *2*, 11–19.
37. Xu, P.; Yang, T.Q. Rheological test and constitutive model identification of rock. *J. Rock Sci. Technol.* **2001**, *20*, 1739–1744.

Disclaimer/Publisher's Note: The statements, opinions and data contained in all publications are solely those of the individual author(s) and contributor(s) and not of MDPI and/or the editor(s). MDPI and/or the editor(s) disclaim responsibility for any injury to people or property resulting from any ideas, methods, instructions or products referred to in the content.